

Density Collapse in Improved Confinement Mode on Tohoku University Helicac

S. Kitajima 1), Y. Tanaka 2), H. Utoh 1), H. Umetsu 1), J. Sato 1), K. Ishii 1), T. Kobuchi 1), A. Okamoto 1), M. Sasao 1), Y. Suzuki 3), M. Yokoyama 3), S. Inagaki 4), K. Nishimura 3), H. Takahashi 3), H. Ogawa 2) and M. Takayama 5)

1) Department of Quantum Science and Energy Engineering, Tohoku University, Sendai, Japan

2) Japan Atomic Energy Agency, Naka, Japan

3) National Institute for Fusion Science, Toki, Japan

4) Kyushu University, Hakozaki, Fukuoka, Japan

5) Akita Prefectural University, Honjyo, Akita 015-0055, Japan

E-mail: sumio.kitajima@qse.tohoku.ac.jp

Abstract. The density collapse was observed in the improved confinement mode sustained by the hot cathode biasing in Tohoku University Helicac (TU-Helicac). The density profiles showed the steep gradient around the core plasma region before the collapse. The steep density profile collapsed accompanied with the bursting high frequency fluctuation ($100 < f < 500$ kHz), which had $m = 2 \sim 3$ poloidal mode number and the frequency agreed well with the $\mathbf{E} \times \mathbf{B}$ plasma rotating frequency. After the collapse the steep gradient in the density profile disappeared and the density outside the core region increased in the level consistent with the decrease of the core region.

1. Introduction

In TU-Helicac, a small helical device, the electrode biasing experiments have been carried on to trigger and achieve an improved confinement mode [1-5] using a hot cathode. In experiments on the TU-Helicac, the role of the radial electric field and the poloidal flow on the transition to improved confinement modes [6-10] has been investigated by electrode-biasing experiments [11]. By negative biasing with the hot cathode, the radial electric fields can be actively controlled by changing the electrode current. The poloidal viscosity was successfully estimated from the $\mathbf{J} \times \mathbf{B}$ external driving force. Here \mathbf{J} and \mathbf{B} are the electrode current and the magnetic field. It was experimentally confirmed that the local maxima in the viscosity play the key role in the L-H transition [12-15]. In a small tabletop machine electrode biasing has a great advantages to study the role of the radial electric field and the poloidal flow in improved confinement modes [16-18].

In this confinement mode assisted by the electrode biasing we observed the density collapse, which occurred periodically around the magnetic axis and accompanied with the bursting high frequency fluctuations [20]. The high frequency fluctuations strongly depended on the plasma poloidal rotation driven by the $\mathbf{J} \times \mathbf{B}$ force, which was externally controlled by the hot cathode biasing. The poloidal Mach number M_p exceeds unity and had $2 \sim 3$ in the biasing experiment in TU-Helicac. In this case the $\mathbf{E} \times \mathbf{B}$ poloidal velocity reached ~ 12 km/s. The collapse did not seem to degrade the overall performance in the improved mode. One of further extended works is to clarify and focus on the physics of the density collapse and the bursting high frequency fluctuations in the ultra high speed poloidal flow ($M_p > 1$). In this paper we report the density collapse and the high frequency fluctuation in the improved confinement mode sustained by the hot cathode biasing on Tohoku University Helicac.

2. Experimental setup and biasing experiments in TU-Heliac

The TU-Heliac is a 4-period heliac (major radius, 0.48 m; average plasma radius, 0.07 m). The heliac configurations were produced by three sets of magnetic field coils: 32 toroidal field coils, a center conductor coil, and one pair of vertical field coils. Three capacitor banks consisting of two-stage pulse forming networks separately supplied coil currents of 10 ms flat top [21]. The target plasma for biasing was He plasma produced by low frequency joule heating ($f = 18.7$ kHz, $P_{\text{out}} \sim 35$ kW). The joule heating power was supplied to one pair of poloidal coils wound outside the toroidal coils [22]. The vacuum vessel was filled with fueling neutral He gas and sealed from the evacuation system before every discharge.

The electrode biasing experiments were carried out using an emissive hot cathode made of LaB₆, which functions as an electron injection source. The LaB₆ hot cathode (diameter, 10 mm; length, 17 mm) was inserted horizontally into the plasma from the low magnetic field side at a toroidal angle $\phi = 270^\circ$ as shown in Fig. 1. The flux surface was bean- or kidney-shape as shown in the A-B poloidal cross-section in Fig.1. The hot cathode was heated by a floating power supply and a negative bias voltage was applied against the vacuum vessel by a voltage-control power supply.

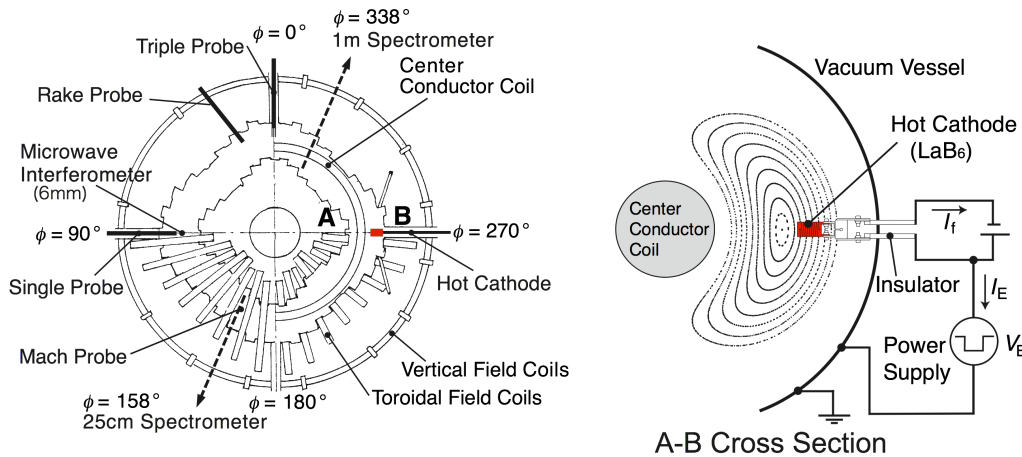


FIG. 1 Experimental set-up. The high speed triple probe was set at a toroidal angle $\phi = 0^\circ$ and the single probe for an event monitor was set at $\phi = 90^\circ$

The radial profiles of electron temperature, density and plasma potential were measured with a high speed triple probe which was located at a toroidal angle $\phi = 0^\circ$, inserted from a low field side and scanned in the equatorial plane. The high speed probe had a wide frequency bandwidth, which resulted from preamplifiers set at the top of the probe shaft installed inside the vacuum vessel [23, 25]. The radial profiles of fluctuation levels in a floating potential and an ion saturation current were also measured with this high speed Langmuir probe. The line density along a vertical chord through the magnetic axis was measured with a 6 mm microwave interferometer at $\phi = 90^\circ$. The radial distributions of a floating potential and an ion saturation current were measured with a rake probe at $\phi = 21.2^\circ$. The visible light emission was monitored using 25 cm and 1 m spectrometers at $\phi = 158^\circ$ and 338° . The plasma flow velocity was measured by a Mach probe at $\phi = 158^\circ$. Figure 2 shows the typical (a) density, (b) temperature and (c) plasma space potential profiles before/during the electrode

biasing measured by the triple probe. The position of the hot cathode were shown by the red rectangle on the horizontal axis and the magnetic axis ($R = 79$ mm) and the last closed flux surface (LCFS, $R = 120$ mm) were pointed by arrows. The typical plasma parameters before biasing were as follows. The electron density on the magnetic axis was $\sim 6 \times 10^{17} \text{ m}^{-3}$ and the electron temperature on the axis was about 20 eV. During biasing the density increased by a factor of 3 \sim 4 and the electron temperature decreased about a half in the core region. The plasma space potential changed the sign from positive to negative and had the steep gradient, which clearly shows that the large radial electric field ($E_r \sim 4 \text{ kV/m}$) were formed by the externally controlled electrode biasing. In this biasing case the $\mathbf{E} \times \mathbf{B}$ poloidal velocity reached $\sim 12 \text{ km/s}$. The average radius of the last closed flux surfaces were about 6 \sim 7 cm and the magnetic field on the axis was 0.3 T.

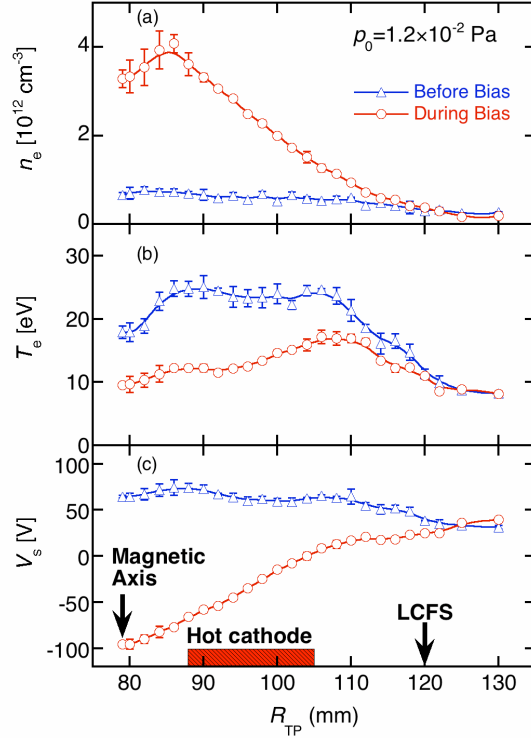


FIG. 2 Typical (a) density, (b) temperature and (c) plasma space potential profiles before/during the electrode biasing measured by the triple probe.

3. Density collapse

The target plasma for the hot cathode biasing was produced by low frequency joule heating ($f = 18.7 \text{ kHz}$). The electron density and temperature at the magnetic axis were $\sim 6 \times 10^{17} \text{ m}^{-3}$ and $\sim 20 \text{ eV}$ measure by a triple probe in the Helium target plasma. The hot cathode made of LaB_6 was negatively biased (-230 V) from the beginning to the end of the discharge. In biased plasma the electron density and temperature at the magnetic axis were $\sim 4 \times 10^{18} \text{ m}^{-3}$ and $\sim 12 \text{ eV}$ respectively as mentioned in section 2. Figure 3 shows the time evolutions of the line density measured by the 6 mm microwave interferometer and the ion saturation current measured by the triple probe and a rake probe

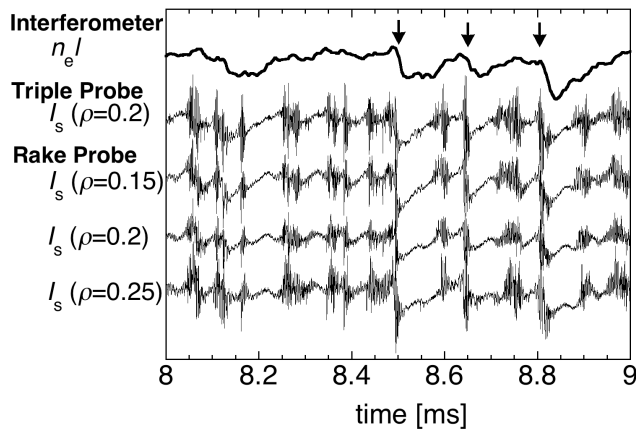


FIG. 3 Time evolutions of the line density measured by the 6 mm microwave interferometer and the ion saturation current measured by the triple probe and a rake probe [24].

measured by the triple probe and the rake probe. We can see the sudden density drops, which are denoted by the arrows, and many small dips in the line density. We can also see the bursting fluctuation signals in the ion saturation current measured by the triple probe ($q = 0.2$) and the rake probe ($q = 0.15, 0.2$ and 0.25) synchronized with the decrease in the line density [24].

In order to measure the density profiles before/after the sudden decrease in the density we measured the profile by the high speed triple probe scanning the radial direction. The decrease in the density was an eruptive event. Therefore we monitored the event by another single probe which was set at a toroidal angle $\phi = 90^\circ$ and fixed at the magnetic axis as shown in Fig. 1. These two probes were set apart from 90° in toroidal angle. Figure 4 shows the typical ion saturation signal measured by the single probe fixed at the magnetic axis. We can see the

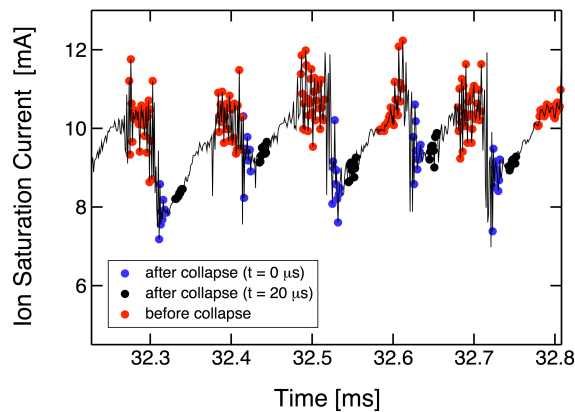


FIG. 4 Typical ion saturation signal (black line) measured by the single probe fixed at the magnetic axis. Red circles denote the data before collapse and blue and black circles denote the data after collapse.

sudden decrease in the ion saturation current (black line) and we also marked the data before the sudden decrease in the probe current (red circles) and the data after the sudden decrease (blue and black circles). We sampled the ion saturation current data measured by the high speed triple probe corresponding to these characteristic points (red, blue and black circles), which were selected through the conditional windows based on the length of repetition period

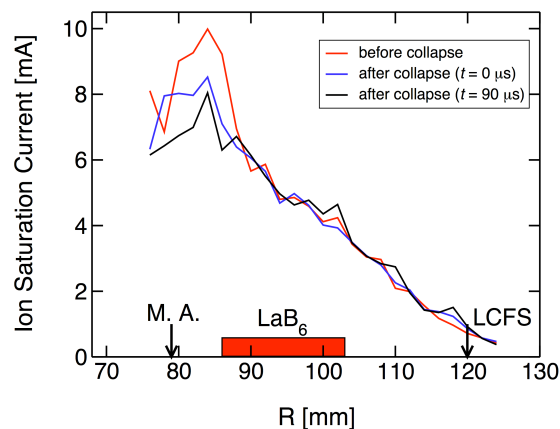


FIG. 5 radial profiles of ion saturation currents measured by the triple probe. Red line shows the profile before the sudden decrease in the density and blue line and black line show the profiles after the decrease ($t = 0 \mu\text{s}$ and $t = 90 \mu\text{s}$)

and the depth of decrease by the data analysis program. This method is one of the *conditional average*. The triple probe was horizontally scanned along the radial direction at the toroidal angle $\phi = 0^\circ$. In Fig. 5 we plot the radial profiles of ion saturation currents measured by the triple probe. These data were selected with the events, which were before the sudden decrease in the density and after the decrease (delay $t = 0 \mu\text{s}$ and $t = 90 \mu\text{s}$ from the sudden decrease) monitored by the single probe. Then the profiles were not measured at the same time. Though the radial profiles were constructed by shot by shot measurements and conditional average, it is clear that before the decrease the profile of the ion saturation current (red line), which corresponds to the plasma density, has the steep gradient in the region of $85 < R < 90 \text{ mm}$ ($0.15 < \varrho < 0.3$). On the other hand after the decrease in the region of $R > 90 \text{ mm}$ ($\varrho > 0.3$) the profile of the ion saturation current (black line) slightly increased accompanied with the decrease in the core plasma region. From the rough estimation the decrease in the volume-integrated density inside the core plasma region was consistent with the increase in the volume-integrated density outside the core plasma region. These profiles reveal the *density collapse*. The condition in which the density collapse appears depends on the biasing condition and the magnetic configuration, especially a rotational transform. The precise dependency is in progress. The over all performance of the confinement hardly degraded in the case of the density collapse discharge, because the region where the collapse appeared was restricted to $R < 90 \text{ mm}$ ($\varrho < 0.3$).

4. Bursting fluctuation

We also observed the *bursting* high frequency fluctuations in the ion saturation current, with which the density collapse accompanied as shown in Fig. 3. Figure 6 shows the time relations between (a) the high frequency fluctuations in the ion saturation current filtered by a high pass filter ($f_{\text{HPF}} = 40 \text{ kHz}$), (b) the radial electric field and (c) the ion saturation current signal filtered by a low pass filter ($f_{\text{LPF}} = 50 \text{ kHz}$). These were measured by the high speed triple probe and the rake probe at $R = 86 \text{ mm}$ ($\varrho = 0.2$). The high frequency fluctuations were bursting with the repetition period $\sim 0.5 < T < 1.5 \text{ ms}$ and the radial electric field E_r suddenly dropped by 80% of the maximum value and the drops in the ion saturation current signal I_s represent the density collapse at $R = 86 \text{ mm}$ ($\varrho = 0.2$) shown in Fig. 5. We can see that the high frequency fluctuation appeared at the sudden radial electric field dips and had the peak amplitude at the ion saturation current drops, which correspond to the density collapse.

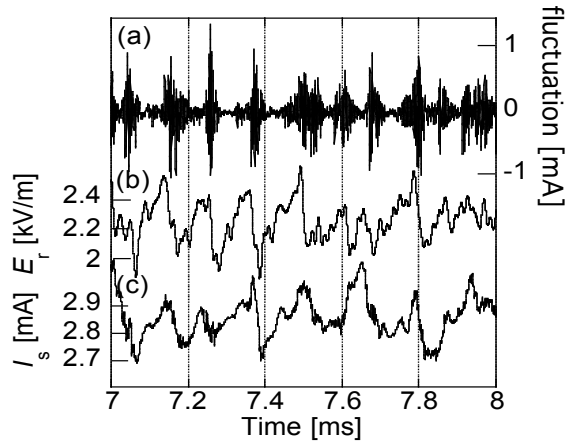


FIG. 6 Time relations between (a) the high frequency fluctuations in the ion saturation current, (b) the radial electric field and (c) the ion saturation current signal.

In order to study the dependance of the bursting high frequency fluctuations in the ion saturation current to the density collapse, we sampled the data before/after the density collapse by the conditional average used in section 3. Figure 7 shows power spectra in the bursting high frequency fluctuations. We can see two spectra in the region of $200 < f < 500 \text{ kHz}$ before collapse (red line), and just after collapse ($t = 0 \mu\text{s}$) the spectra had broader profiles and at $t = 20 \mu\text{s}$ delay from the collapse the power of the spectra decreased in the

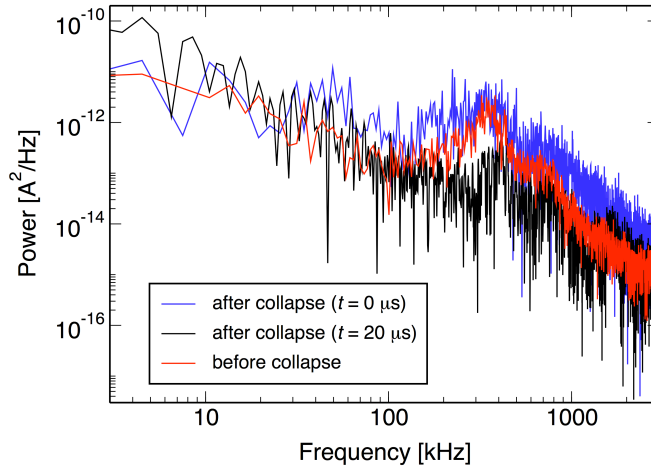


FIG. 7 Power spectra in the bursting high frequency fluctuations

region of $100 < f < 2000$ kHz. These were consistent with the time evolution of the bursting fluctuations shown in Fig. 6. The sampling data lengths of the triple probe signals at each event “before collapse”, “just after collapse ($t = 0 \mu\text{s}$)” and “at $t = 20 \mu\text{s}$ delay from the collapse” were $30 \mu\text{s}$, $20 \mu\text{s}$ and $20 \mu\text{s}$ respectively. These spectra were measured at $R = 86$ mm ($\varrho = 0.2$).

The radial distributions of the power spectra of the high frequency fluctuations was shown in Figs. 8 and 9. Figure 8 (a) corresponds to the data before collapse (red lines in Fig. 7) and Fig.

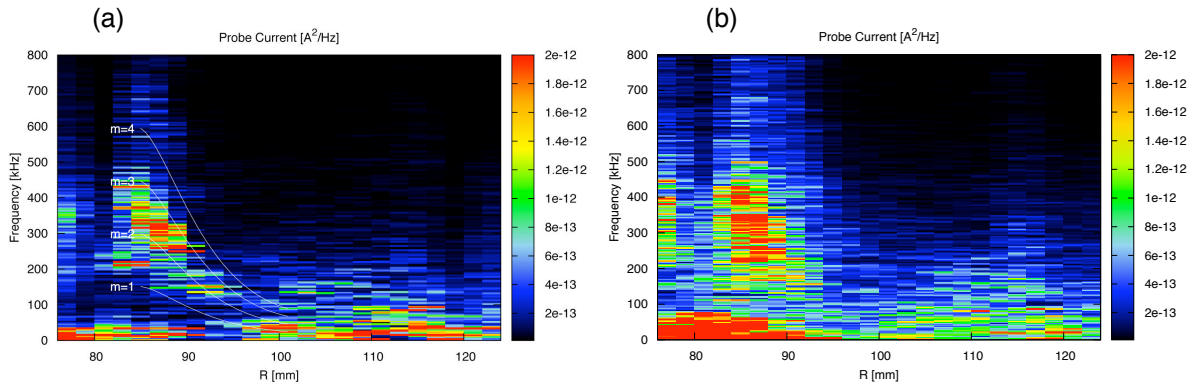


FIG. 8 Radial distributions of the power spectra (a) before collapse and (b) after collapse $t = 0 \mu\text{s}$. White lines in (a) represent the $\mathbf{E} \times \mathbf{B}$ rotating frequency

8 (b) corresponds to the data after collapse $t = 0 \mu\text{s}$ (blue lines in Fig. 7). The high frequency fluctuations had the spectrum in the region of $100 < f < 500$ kHz and the peak frequency of the spectrum was decreasing with increase in the radial position. The white lines in Fig. 8 (a) were the $\mathbf{E} \times \mathbf{B}$ rotating frequency calculated from

$$f_{E \times B} = \frac{mE_r}{2\pi \langle r \rangle B}, \quad (1)$$

here E_r , $\langle r \rangle$ and m are the radial electric field, the averaged minor radius and the integer that corresponds to the poloidal mode number. The radial electric field E_r was estimated from the space potential measured by the triple probe. The lines for $m = 2 \sim 3$ agreed well with the peak frequency radial distribution of the spectrum. It shows that the high frequency fluctuations in connection with the density collapse strongly depended on the $\mathbf{E} \times \mathbf{B}$ plasma poloidal rotation driven by the hot cathode biasing and had the $m = 2 \sim 3$ poloidal mode number. This confirms that the bursting fluctuation frequency tightly depends on the high

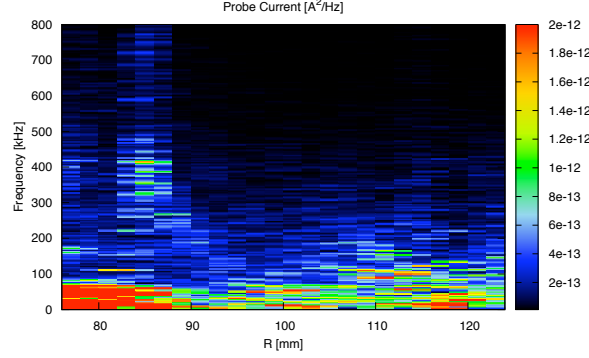


FIG. 9 Radial distribution of the power spectra at $t = 20 \mu\text{s}$ delay from the collapse

speed poloidal flow. In this biasing case the $\mathbf{E} \times \mathbf{B}$ poloidal velocity reached ~ 12 km/s. After collapse (Fig. 8 (b)) the high frequency fluctuations had the broader spectrum than that before collapse. And after $t = 20 \mu\text{s}$ delay from the collapse the power of the spectra as shown in Fig. 9 extremely decreased in the region of $100 < f < 500$ kHz. These show that the bursting high frequency fluctuations in the ion saturation current grew with the increase in the core density $85 < R < 90$ mm ($0.15 < \varrho < 0.3$) and had the peak amplitude at the ion saturation current drops, which correspond to the density collapse.

We arranged the power of fluctuation in ion saturation current in order to study the dependence to the density gradient ∇n . We substituted the ion saturation gradient ∇I_s at $r = 86$ mm ($\varrho = 0.2$) for the density gradient ∇n . Figure 10 shows the relation between power spectra and the density gradient. The spectrum in the region of $350 < f < 450$ kHz increased according to the increase in the gradient in the region $\nabla I_s > 4.5 \times 10^{-4}$ [A/m] and the new spectrum appeared in the region of $150 < f < 250$ kHz at $\nabla I_s > 5.5 \times 10^{-4}$ [A/m]. This confirms that the

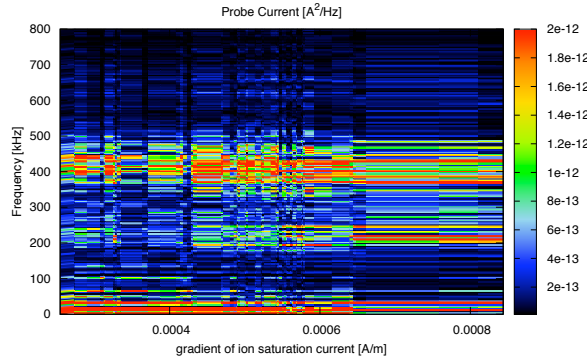


FIG. 10 Relation between power spectra and the density gradient

bursting high frequency fluctuations in the ion saturation current grew with the increase in the density gradient in the region of $85 < R < 90$ mm ($0.15 < \rho < 0.3$).

5. Summary

We observed the density collapse and the bursting high frequency fluctuations in the plasma which had ultra high speed poloidal flow ($M_p > 1$) in TU-Heliac. The ultra high speed poloidal flow was sustained by the hot cathode biasing. We adopted the conditional average to analyze the ion saturation signals and showed the availability of this method. The density profiles showed the steep gradient around the core plasma region before the collapse. The steep density profile collapsed accompanied with the bursting high frequency fluctuation ($100 < f < 500$ kHz), which had $m = 2 \sim 3$ poloidal mode number and the frequency agreed well with the $\mathbf{E} \times \mathbf{B}$ plasma rotating frequency. This confirms that the bursting fluctuation frequency tightly depends on the high speed poloidal flow. After the collapse the steep gradient in the density profile disappeared and the density outside the core region increased in the level consistent with the decrease of the core region.

Acknowledgments

This work was supported by a Grant-in-Aid from the Ministry of Education, Science and Culture of Japan (No 17360439) and in part by the LHD Joint Planning Research programme at the National Institute for Fusion Science.

References

- [1] Wagner F. *et al* 1982 *Phys. Rev. Lett.* **49** 1408.
- [2] Burrell K.H. *et al* 1987 *Phys. Rev. Lett.* **59** 1432.
- [3] Kotschenreuther M. *et al* 1995 *Phys. Plasmas* **2** 2381.
- [4] Erckmann V. *et al* 1993 *Phys. Rev. Lett.* **70** 2086.
- [5] Toi K. *et al* 1996 *Plasma Phys. Control. Fusion* **38** 1289.
- [6] Itoh S.-I., Itoh K. 1988 *Phys. Rev. Lett.* **60** 2276.
- [7] Shaing K.C., Crume J.E.C. Jr. 1989 *Phys. Rev. Lett.* **63** 2369.
- [8] Shaing K.C. 1993 *Phys. Fluids B* **5** 3841.
- [9] Shaing K.C. 1996 *Phys. Rev. Lett.* **76** 4364.
- [10] Rozhansky V., Tendler M. 1992 *Phys. Fluids B* **4** 1877.
- [11] Inagaki S. *et al* 1997 *Japan. J. Appl. Phys.* **36** 3697.
- [12] Kitajima S. *et al* 2006 *Nucl. Fusion* **46** 200.
- [13] Kitajima S. *et al* 2006 *Plasma Phys. Control. Fusion* **48** A259.
- [14] Kitajima S. *et al* 2008 *Nucl. Fusion* **48** 035002.
- [15] Takahashi H. *et al* 2006 *Plasma Phys. Control. Fusion* **46** 39.
- [16] Dahi H., Talmadge J.N., Shohet J.L. 1998 *Phys. Rev. Lett.* **80** 3976.
- [17] Takahashi H. *et al* 2003 *J. Plasma Fusion Res. Ser.* **6** 366.
- [18] Kitajima S. *et al* 2006 *Fusion Sci. Technol.* **50** 201.
- [19] Utoh, H. *et al* 2006 *Fusion Sci. Technol.* **50** 434.
- [20] Tanaka Y. *et al* 2006 *Plasma Phys. Control. Fusion* **48** A285.
- [21] Kitajima S. *et al* 1991 *Japan. J. Appl. Phys.* **30** 2606.
- [22] Kitajima S. *et al* 2001 *J. Plasma Fusion Res. Ser.* **4** 391.
- [23] Tanaka Y. *et al* 2007 *Plasma Fusion Res.* **2** S1090.
- [24] Tanaka Y. *et al* 2008 *Plasma Fusion Res.* **3** S1055.